Title

Targeting uPAR with Antagonistic Recombinant Human Antibodies in Aggressive Breast Cancer

Journal

Cancer Research, 73(7)

ISSN

0008-5472

Authors

LeBeau, Aaron M
Duriseti, Sai
Murphy, Stephanie T
et al.

Publication Date

2013-04-01

DOI

10.1158/0008-5472.can-12-3526

Peer reviewed

Published in final edited form as:
Cancer Res. 2013 April 1; 73(7): 2070–2081. doi:10.1158/0008-5472.CAN-12-3526.

Targeting uPAR with Antagonistic Recombinant Human Antibodies in Aggressive Breast Cancer

Aaron M. LeBeau[1,2,6], **Sai Duriseti**[3,6], **Stephanie T. Murphy**[2], **Francois Pepin**[4], **Byron Hann**[5], **Joe W. Gray**[4], **Henry F. VanBrocklin**[2], and **Charles S. Craik**[1]

[1]Department of Pharmaceutical Chemistry, University of California, San Francisco, San Francisco, California USA

[2]Center for Molecular and Functional Imaging, Department of Radiology and Biomedical Imaging, University of California, San Francisco, San Francisco, California USA

[3]Graduate Group in Biophysics, University of California, San Francisco, San Francisco, California USA

[4]Life Sciences Division, Lawrence Berkeley National Laboratory, Berkeley, California USA

[5]Preclinical Therapeutics Core, UCSF Helen Diller Family Comprehensive Cancer Research Center, University of California, San Francisco, San Francisco, California, USA

Abstract

Components of the plasminogen activation system (PAS) which are overexpressed in aggressive breast cancer subtypes offer appealing targets for development of new diagnostics and therapeutics. By comparing gene expression data in patient populations and cultured cell lines, we identified elevated levels of the urokinase plasminogen activation receptor (uPAR, *PLAUR*) in highly aggressive breast cancer subtypes and cell lines. Recombinant human anti-uPAR antagonistic antibodies exhibited potent binding *in vitro* to the surface of cancer cells expressing uPAR. *In vivo* these antibodies detected uPAR expression in triple negative breast cancer (TNBC) tumor xenografts using near infrared (NIR) imaging and ^{111}In single-photon emission computed tomography (SPECT). Antibody-based uPAR imaging probes accurately detected small disseminated lesions in a tumor metastasis model, complementing the current clinical imaging standard ^{18}F-fluorodeoxyglucose (FDG) at detecting non-glucose-avid metastatic lesions. A monotherapy study using the antagonistic antibodies resulted in a significant decrease in tumor growth in a TNBC xenograft model. Additionally, a radioimmunotherapy (RIT) study, using the anti-uPAR antibodies conjugated to the therapeutic radioisotope ^{177}Lu, found that they were effective at reducing tumor burden *in vivo*. Taken together, our results offer a preclinical proof of concept for uPAR targeting as a strategy for breast cancer diagnosis and therapy using this novel human antibody technology.

Address Correspondence to: Henry F. VanBrocklin, Ph.D., Department of Radiology and Biomedical Imaging, University of California, San Francisco, 185 Berry Street, Suite 350, San Francisco, CA, 94143-2280, Phone: (415) 353-4569, Fax: (415) 514-8242 or Charles S. Craik, Ph.D., Department of Pharmaceutical Chemistry, University of California, San Francisco, 600 16th St., Box 2280, San Francisco, CA 94143-2280, Phone: (415) 476-8146, Fax: (415) 502-8298.
[6]These authors contributed equally to this work.
Current address for Joe W. Gray: Department of Biomedical Engineering, Oregon Health and Science University, Portland, Oregon USA.

The authors disclose no potential conflicts of interest

Keywords

breast cancer; imaging tumor progression and metastasis; non-invasive imaging; novel anti-tumor agents; new targets

Introduction

Breast cancer is a remarkably heterogeneous disease comprised of multiple subtypes, each representing a distinct biological signature that responds to unique therapeutic regimens (1, 2). Therapeutics that target specific subtypes, such as trastuzumab (Herceptin) in the HER2 positive subtype, have been effective at treating primary and metastatic breast cancer, but ultimately drug resistance and clinical relapse occur in a majority of patients (3, 4). Despite the recent FDA approval of several new drugs for the treatment of breast cancer, therapeutic options for metastatic breast cancer are few (5). Once cells from the primary tumor metastasize to the bone and soft tissue, the primary goal of therapy is palliative (6). Molecular targets of aggressive subtypes are needed for the treatment and evaluation of the disease. Agents directed towards these targets can be utilized as diagnostic probes or targeted therapeutics. Diagnostic imaging probes would allow for the non-invasive identification of aggressive tumors that are non-responsive to standard chemotherapeutics, and allow patients to receive alternative therapeutic options sooner. If the target is reflective of tumor viability, metastatic lesions can be identified earlier and response to therapy can be dynamically quantified. Furthermore, therapeutics directed towards molecular targets could reduce patient morbidity associated with non-targeted systemic therapies, and ultimately prolong survival.

The PAS presents several molecular targets that can be exploited for diagnostic and therapeutic purposes in metastatic breast cancer. The over-expression of the serine protease urokinase plasminogen activator (uPA) and its receptor uPAR have been found to contribute to the aggressive phenotype of a number of cancers (7, 8). In breast cancer, high levels of uPA and its cognate inhibitor plasminogen activator inhibitor-1 (PAI-1) in tumor tissue were found to correlate with poor clinical prognosis and were predictors of tamoxifen resistance (9, 10). Several investigators found that uPAR expression in breast tissue is directly correlated with an aggressive tumor phenotype and low disease-free survival. uPAR expression has been documented in triple-negative breast cancer (TNBC), tamoxifen refractory breast cancer and in a subset of Her2-positive breast tumors, all of which are classified as aggressive (11–13). *In vitro* over-expression of uPAR in breast cancer cells was able to induce the epithelial-to-mesenchymal transition (EMT), suggesting that uPAR over-expression can promote an aggressive phenotype (14). Due to its accessibility on the surface of cancer cells, uPAR is of particular interest as a molecular target for breast cancer.

The development of human recombinant anti-uPAR antagonistic antibodies, by panning a fragment-antigen binding (Fab) phage display library against recombinant human uPAR, has been previously reported (15). Two antibodies, 3C6 and 2G10, were characterized for their ability to inhibit uPAR function. Using *in vitro* methods, 3C6 was found to prevent the association of uPAR with β1 integrin, while 2G10 prevented uPA's association with uPAR. Both antibodies were found to be selective for human uPAR and did not cross-react with murine uPAR. In this report, we document the use of 3C6 and 2G10 as molecular imaging and therapeutic agents in preclinical models of aggressive breast cancer. 3C6 and 2G10 IgGs detected uPAR expression in breast cancer cell-derived orthotopic xenograft tumors, and in disseminated lesions of cardiac dissemination model (CDM) mice by NIR optical imaging and, the clinically relevant nuclear imaging modality, SPECT. The ^{111}In-labeled anti-uPAR IgG SPECT probes complemented the clinical imaging standard ^{18}FDG positron emission

tomography (FDG-PET) by detecting lesions missed by FDG-PET. In a high dose monotherapy study, both 2G10 IgG and 3C6 IgG resulted in decreased tumor growth with no growth observed in the 2G10 IgG treated group. A radioimmunotherapy (RIT) study with ^{177}Lu-2G10 IgG, resulted in complete tumor regression, suggesting uPAR as a viable therapeutic target for breast cancer. This investigation demonstrates that high uPAR expression is a prominent clinical feature of aggressive breast cancer, corroborating *in vitro* cell studies, and that our antibodies allow uPAR targeting for diagnostic and therapeutic purposes.

Materials and Methods

Cell Culture

Human breast cancer cell lines MDA-MB-231, MDA-MB-435, MDA-MB-436, MDA-MB-453, MDA-MB-468, BT-549, SK-Br3 and MCF-7 were purchased from American Type Culture Collection (ATCC) and were maintained in their respective recommended media, supplemented with 10% FBS, 100 U/ml penicillin, and 100 μg/ml streptomycin at 37°C. The drug resistant cell lines MCF-7 TamR, MCF-DoxR, MDA-MB-231 TaxR and MDA-MB231 DoxR were a generous gift from Dr. Laura L. Murphy (Southern Illinois University School of Medicine) and were cultured as mentioned above. Human mammary epithelial cells (HMEC) were purchased from Lonza and cultured using the MEGM™ BulletKit™. The cell lines were authenticated using short-tandem repeat profiling provided by the vendor.

uPAR mRNA expression analysis in the NKI dataset

Using the Netherlands Cancer Institute (NKI) dataset, which reports mRNA levels for 24,498 genes in 295 women with breast cancer, uPAR mRNA levels were assessed and their significance in several breast cancer subtypes was compared (16) The data were stratified according to previously reported methods (17). Patients diagnosed with basal (BLBC), Her2 (ERBB2), Luminal A, Luminal B, or Normal-like breast cancer were grouped. A non-parametric Wilcoxian t-test was performed to determine which group had significant uPAR mRNA. uPAR mRNA levels in patients falling under the TNBC subtype with all other breast cancer subtypes were compared.

uPAR gene expression analysis in breast cancer cell lines

RNA was prepared from each cell line (~ 2×10^6 cells/cell line) using an RNEasy kit (Qiagen). Following RNA isolation, each sample was treated with Turbo DNA-free (Ambion) to remove any residual DNA. RNA was synthesized to cDNA using the High Capacity RNA-to-cDNA kit (Applied Biosystems). For each gene, Taqman qPCR was performed in quadruplicate using the Taqman Universal PCR Master Mix (Applied Biosystems). The following Taqman Gene Expression Assay probes were used: uPAR – Hs00182181_m1 PLAUR, uPA – Hs01547054_m1 PLAU, PAI-1 Hs01126606_m1 and 18s ribosomal 1 (reference gene) Hs03928985_g1 RN18S1. All qPCR was performed on an ABI 7300 Real Time PCR system instrument. qPCR raw data (Ct) for each sample was normalized to the reference gene. Data was analyzed using the comparative Ct method (fold change = $2^{-\Delta\Delta Ct}$) with data normalized to the negative control cell line, MDA-MB-453.

Fab and IgG production

2G10 (λ light chain) and 3C6 (κ light chain) Fabs and IgG1s were produced as previously described (15) and the IgGs were purified on a Protein A FF column (GE Life Sciences), and then on an S75 HiLoad Prep column. A11, isotype matched control IgG1 in this study, was expressed and purified as originally described (18).

Flow cytometry

MDA-MB-231, MCF-7 and HMEC cells were washed with DPBS and harvested with TrypLE (Gibco). 1×10^6 cells were incubated with 10 nM 2G10 or 3C6 IgG for 20 minutes at 4°C, followed by FITC-labeled anti-human IgG antibody (BD) for another 20 minutes at 4°C. Stained samples and controls were assayed on a BD Facscalibur. In the experiments for determining apparent dissociation constants for MDA-MB-231 cells, cells were harvested as described, and separated into 1×10^5 aliquots. The antibody constructs, 2G10 and 3C6 (Fab and IgG) and A11 isotype control IgG, were incubated at 4°C with the cells for 90 min. For apparent K_D calculations, all cells were incubated with their defined antibody concentration for 12 hours in DMEM-H21 at 4°C to account for the attenuated k_{off} of IgG-treated samples affecting calculated apparent K_D. Fab samples were also incubated for one hour to ensure that data for samples incubated for longer periods were not skewed by dead cells (98% cell viability after one hour, versus 95% viability after 12 hours, data not shown). Samples and controls were probed with a phycoerythrin-labeled anti-human Fc_γ and assayed on an LSRII flow cytometer (BD). All concentrations were done in triplicate.

Surface Plasmon Resonance

Soluble uPAR was immobilized on a CM5 chip via EDC/NHS chemistry, where exposed lysines on suPAR's surface were covalently linked to the dextran surface. 2G10 and 3C6 Fab samples were made at 1, 4, 16, 64, and 256 nM for analysis. 2G10 and 3C6 IgG samples were made at 0.0390625 nM, 0.15625, 0.625, 2.5, 10, 40, and 160 nM for analysis. SPR experiments were conducted in a Biacore T100 apparatus. All samples were flown over the chip surface at 30μls/min for 30 seconds, followed by a 120 second dissociation phase, and removed with Glycine pH 2.5 for 30 seconds. Response curves were evaluated in the BiaEvaluation software. For determination of the dissociation constants, a 1:1 Langumurian best-fit binding model was employed for both Fab and IgG binding curves.

Animal Models for imaging

The animal work was performed in accordance with a UCSF Institutional Animal Care and Use Committee protocol and was performed by the Preclinical Therapeutics Core at UCSF. Six to seven-week-old nu/nu mice were purchased from Taconic Farms. Nude mouse xenografts were generated by subcutaneous injection of each cell line (1×10^6 cells/ml; 100 μl per site/mouse) in the mammary fat pad of the mouse. MCF-7 mice were subcutaneously implanted with a slow-release estrogen pellet (0.8mg of 17β-estradiol) in the contralateral flank. The intracardiac dissemination model was generated using the previously described method (19).

In vivo molecular imaging

Optical—IgGs were labeled with AlexaFluor 680 for NIR imaging using a previously published protocol (18). Images were collected in fluorescence mode on anIVIS 50 (Caliper/Xenogen) using Living Image 2.50.2 software at 24 hour intervals out to 120 hours. Using the software, region of interest measurements were made and the fluorescence emission images were normalized to reference images and the unitless efficiency was computed. For bioluminescence imaging, the mice were injected with intraperitoneally with D-luciferin (150 mg/kg body weight). Images were acquired 10 min after the injection of D-luciferin and the total flux (p s-1) in the region of interest was measured.

SPECT/CT—The chelate group for ^{111}In, 1,4,7,10-Tetraazacyclododecane-1,4,7,10-tetraacetic acid N-hydroxysuccinimide ester (DOTA-NHS) (Macrocyclics), was attached to lysine residues on the IgG using a 25:1 molar excess of chelate in a 0.1 M $NaHCO_3$, pH 9.0 buffer with an antibody concentration of 6 mg/ml. After two hours of labeling at room

temperature, the antibody-DOTA conjugate was FPLC purified to remove unreacted DOTA-NHS. For ^{111}In radiolabeling, $^{111}InCl_3$ was purchased from Perkin Elmer (Shelton, CT). To radiolabel the IgG, 50 μg of DOTA conjugate in 0.2 M ammonium acetate (pH 6.0) was incubated with 12μl of $InCl_3$ (2.10 mCi) in 0.1 N HCl for 60 minutes at 40°C. Labeled products were purified using a PD-10 column pre-equilibrated with PBS buffer. Labeling efficiency and purity of the product were determined using thin-layer chromatography. For mouse imaging, 2.5 – 5.0 μg of probe, corresponding to 275 – 360 μCi of activity, were injected into the tail vein. The mice were imaged at 24 hour intervals out to 120 hours using a Gamma Medica Ideas XSPECT SPECT/CT imaging system. Reconstructed data was analyzed with AMIDE and AMIRA software.

Probe quality control—After labeling with AlexaFluor 680, DOTA, ^{111}In and ^{177}Lu, the antibodies were tested for their ability to retain affinity for uPAR using ELISA. Recombinant soluble uPAR was immunosorbed onto a Nunc Maxisorp plate. Labeled antibodies and unlabeled controls were added to wells, and binding was probed with a biotinylated anti-Fc receptor antibody, followed with an avidin-HRP conjugate. Reactions were stopped with sulfuric acid after five minutes and read on a UV-Vis microplate reader. Values (done in quadruplicate) for wells with the respective labeled antibody were averaged and normalized by the average measurement for the wells probed with unlabeled antibody. Decreased affinity was never observed for any of the labeled antibodies.

FDG PET/CT—PET scans were performed on a PET/CT scanner (Inveon, Siemens Healthcare, Malvern, PA). Mice fasted overnight were injected intravenously with 150–200 μCi FDG. PET images were acquired 50 minutes post-injection in one 600 second frame. CT images were acquired in 120 projections of continuous rotation to cover 220 degrees with x-ray tube operating at 80 kVp, 0.5 mA, and 175 ms exposure time. The mice were kept warm on a heating pad to minimize radiotracer accumulation in non-tumor tissues. PET images were reconstructed using a manufacturer-provided ordered subsets expectation maximization (OS-EM) algorithm resulting in a 128×128×159 matrices with a voxel size of 0.776×0.776×0.796 mm^3. The data was analyzed with AMIRA software.

Biodistribution study

Mice (n = 4/time point) bearing MDA-MB-231 xenografts between 120 – 250 mm^3 in volume were injected with 25 μCi (2.5 μg) of ^{111}In-2G10 and ^{111}In-3C6. At 24, 48 and 72hrs, the animals were euthanized for analysis in accordance with UCSF Animal Care and Use Committee guidelines. Mice (n = 3/xenograft) bearing MDA-MD-231 (uPAR-), MCF-7, MCF-7 TamR and MDA-MB-435 xenografts 231 xenografts between 120 – 250 mm^3 in volume were injected with 25 μCi (2.5 μg) of ^{111}In-2G10 and ^{111}In-3C6 were euthanized for analysis at 72hrs. Blood was collected by cardiac puncture. The tumor, heart, lung, liver, spleen, kidneys, and muscle were harvested, weighed and counted in an automated γ-counter (Wizard2; Perkin Elmer). The percentage injected dose per gram (% ID/g) of tissue was calculated by comparison with standards of known radioactivity. The uPAR knockout cell line was generated using uPAR shRNA Plasmid (h): sc-36781-SH from Santa Cruz. Transfection was performed with a lentiviral particle according to the manufacturer's protocol. Following puromycin treatment, clones were selected using flow cytometry with AlexaFluor 488 labeled 2G10 IgG. Gene expression of the clone used for the xenograft study was analyzed using qPCR and flow cytometry.

In vitro and *in vivo* therapeutic studies

The matrigel invasion and clonogenic survival assays were performed as previously described (15, 20). For the MTT assay, 2,000 cells were plated in 96 well format. After 24hrs, the cells were incubated with 2.5μg of unlabeled antibodies or 2.5μg of antibodies

labeled with ^{177}Lu at activities of 50μCi and 25μCi. The ^{177}Lu-antibodies were prepared under the same conditions as the ^{111}In-antibodies for imaging. The cells were incubated for 96hrs with the radiolabeled antibodies and then the cell viability was determined using an MTT assay kit (Promega) according to the manufacturer's protocol. For the *in vivo* studies, the animal models were generated by the Preclinical Therapeutics Core at UCSF. Briefly, suspended tumor cells in a buffered solution of 1.0×10^6 cells/100μl were injected into the subcutis of the mammary fat pad of 6 to 7-week-old nude female mice. When the mean tumor volume of mice with established palpable tumors were measured to be > 100 mm^3, the mice were randomized into different treatment groups (n = 10/arm). When the study began at Day 0, tumor volumes of the animals were between 75 –200 mm^3. The mice were treated with 30mg/kg of 2G10, 3C6, A11 and saline at days 3, 10, 17 and 24. For the RIT study, randomized MDA-MB-231 xenograft mice (n=10/arm), with tumor volumes > 100mm^3, were treated with ^{177}Lu-2G10 (75μCi, 2.5μg/dose), ^{177}Lu-EDTA (75μCi), saline and 2G10 (4mg/kg) at days 7 and 21. Mice were weighed weekly and the tumor volumes were calculated using the formula: volume = 0.5236 × L × W × H. Animals were removed from the study and sacrificed when tumor volumes were > 1000mm^3, in accordance with our animal protocol.

Statistical analysis

On box plots, the highest horizontal line represents the highest value in a group, the topmost section represents the top quartile, the part of the white box represents the second highest quartile, the dark horizontal bar represents the median, the bottom part of the white boxes represent the second to lowest quartile, the lowermost quartile represents the lowest quartile, and the lowest horizontal line represents the lowest value in the group. In all other graphs, error bars represent means ± standard deviation.

Results

uPAR Expression is Associated with Aggressive Breast Cancer *In Vivo* and *In Vitro*

Using the NKI dataset, uPAR mRNA levels were compared between patients of different breast cancer subtypes (16, 17). As shown in Fig. 1a, the basal-like breast cancer (BLBC) subtype was found to have the highest uPAR mRNA levels among the subtypes. Knowing that BLBCs often exhibit a triple-negative (TN) phenotype (absence of the Her2, estrogen receptor, and progesterone receptor), the correlation of TN status with uPAR mRNA levels was evaluated. A non-parametric Wilcoxian t-test was used to analyze uPAR levels between BLBC and other subtypes, or TN breast cancer (TNBC) and other subtypes (21–23). While the correlation between uPAR mRNA levels and BLBC was strong ($P = 6\times10^{-8}$, Fig. 1a) the correlation between uPAR mRNA levels and TNBC was stronger ($P = 1.2\times10^{-10}$, Fig. 1b). Longitudinally, uPAR mRNA levels were further correlated with poor clinical prognosis and an earlier recurrence of cancer progression.

Quantitative PCR (qPCR) was used to survey breast cancer cell lines for PAS expression. (Fig. 1c). The aggressive TNBC cell line MDA-MB-231 and its drug-resistant variants had the highest expression of PAS proteins. The TNBC cell lines MDA-MB-436 and BT549 also expressed significant levels of PAS proteins compared to Luminal subtype cell lines (SK-Br3 and MCF-7). Tamoxifen-resistant MCF7 (MCF-7 TamR, which have undergone EMT, are more aggressive than the parental line, and recreate Luminal A tamoxifen-resistant breast cancer *in vivo*) expressed high mRNA levels of the PAS proteins (24). Flow cytometry confirmed that mRNA levels correlated with higher surface uPAR. As shown in Fig. 1d, 3C6 and 2G10 IgG bound to MDA-MB-231 cells more strongly than to either MCF-7 or HMEC cells,, which correlates with the observed high uPAR mRNA levels. A11 IgG, a matched isotype control IgG, did not bind to the cell lines surveyed. Dissociation

constants for the Fabs and IgGs were obtained by flow cytometry by titrating the antibody to construct binding isotherms. The Fabs had lower affinities for MDA-MB-231 cells, 95 nM and 800 nM for 2G10 and 3C6 Fabs, compared to their IgG forms, with values of 53 nM and 96 nM for 2G10 and 3C6, respectively (Suppl. Fig. S1 and Table 1). Dissociation constants for the Fabs and IgGs were also obtained using surface plasmon resonance (SPR). SPR using soluble recombinant uPAR yielded values of 10 nM and 50nM for 2G10 and 3C6 Fab, respectively, while the bivalent affinities of the IgGs were markedly lower at 2 pM and 230 pM for 2G10 and 3C6 (Table 1). The high affinities of the IgGs made them appropriate candidates for *in vivo* studies.

2G10 and 3C6 Preferentially Accumulate in MDA-MB-231 Orthotopic Xenograft Tumors *In Vivo*

NIR optical was initially used to investigate the specific localization of the antibodies to uPAR expressing xenografts and to acquire pharmacokinetics leading to the informed selection of the appropriate isotope for nuclear imaging. AlexaFluor 680 labeled antibodies were injected into bilateral orthoptopic MDA-MB-231 and MCF-7 xenograft umor-bearing mice and serially imaged. 2G10 and 3C6 exhibited strong localization to the uPAR expressing MDA-MB-231 xenograft (Fig. 2). Specificity was evident 48 hours post-injection, and persisted well out to 96 hours. NIR probe localization was neither observed in the uPAR- MCF-7 xenografts nor in MDA-MB-231 xenograft mice injected with scrambled isotype control AlexaFluor 680-labeled IgGs (Suppl. Fig. S2).

The nuclear imaging modality SPECT was used to assess the extent of 3D probe localization and pharmacokinetics *in vivo*. For SPECT imaging, the IgGs were labeled with a 1,4,7,10-tetraazacyclododecane-1,4,7,10-tetraacetic acid (DOTA) chelate derivative. The DOTA-labeled IgGs were chelated with the long lived isotope ^{111}In and administered intravenously to MDA-MB-231 and MCF-7 xenograft mice. In the reconstructed SPECT/CT data, ^{111}In-2G10 and ^{111}In-3C6 demonstrated pronounced tumor localization and retention in the MDA-MB-231 xenograft 72 hours post-injection (Fig. 3a). No localization was observed in the MCF-7 xenografts injected with ^{111}In- 2G10 (Fig. 3b). The time activity curves for ^{111}In-2G10 and ^{111}In-3C6 found tumor uptake at its zenith 72 hours post-injection (Suppl. Fig. 3.). A biodistribution study performed at 24hr, 48hr and 72hr, confirmed high tumor uptake for both probes (Fig. 3c). At 72 hours, the %ID/g values were 53.2% and 31.8% for ^{111}In-2G10 and ^{111}In-3C6, respectively (Fig. 3c). ^{111}In-2G10 had more favorable tumor-to-blood (T/B) and tumor-to-muscle (T/M) ratios compared to ^{111}In-3C6 with values of 12 and 114 for ^{111}In-2G10 and 4, and 36 for ^{111}In-3C6. MDA-MB-231 (uPAR-) xenografts, with uPAR expression knocked-out using shRNA, did not demonstrate significant tumor retention of the probes at 72hrs post-injection nor did the uPAR negative cells lines MCF-7 and MDA-MB-435 (Fig 3d). MCF-7 TamR, with high uPAR mRNA expression, had tumor uptake values for the probes nearly identical to the MDA-MB-231 xenografts at 72hrs (Fig 3d). At 120 hours post-injection, ^{111}In-2G10 cleared from all secondary tissues and a scintigraphic signal was only observed in the tumors (Suppl. Movie M1). A subsequent pharmacokinetics study found the *in vivo* half-lives of ^{111}In-2G10 and ^{111}In-3C6 to be 9.1 days and 5.8 days (Suppl. Fig. S4).

2G10 and 3C6 Identify MDA-MB-231 CDM Model Lesions *In Vivo*

Further evaluation of 2G10 and 3C6 was conducted in MDA-MB-231 CDM models to test probe localization in smaller, dispersed lesions. Intracardiac injection of MDA-MB-231 cells in mice generated tumors analogous to breast cancer metastases in humans (19). Since the MDA-MB-231 cells were engineered to stably express luciferase, the formation of the micro-metastases was followed with bioluminescence imaging (BLI). 3C6 and 2G10 were potent imaging agents in the CDM model, able to detect lesions millimeters in size (Fig. 4

and Suppl. Fig. S5). The SPECT signal from 3C6 co-registered with the observed BLI signal, resolving a 15.9 mm^3 osteolytic lumbar lesion (Fig. 4a). 2G10 identified lesions in the ilium (53 mm^3) and knee (14.3 mm^3) that co-registered with BLI (Fig. 4b). 2G10 detected a number of osseous and soft-tissue lesions, including a 63 mm^3 lesion at the base of the skull (Fig. 4c). The lesions depicted in Figure 4 were found to be non-FDG avid. Interestingly, the tumor shown in the reconstructed data of Figure 4c demonstrated FDG uptake in areas surrounding the tumor, but not in the tumor itself. Fifteen mice, representing 36 BLI detectable lesions, were imaged with the uPAR probes and FDG. Non-FDG-avid tumors imaged by the uPAR probes represented 34 out of 36 lesions (94%), while the remaining two demonstrated exclusive FDG uptake and were not detectable by the uPAR probes (Suppl. Fig S8).

Anti-uPAR Antibodies Affect Tumor Growth *In Vivo*

Encouraged by the imaging data, the therapeutic benefit of the antibodies was next investigated *in vitro* and *in vivo*. Any putative anti-tumor effects of 2G10 or 3C6 on cells were initially investigated using the antibodies to inhibit migration of MDA-MB-231 cells in a Matrigel invasion assay. Both antibodies were potent inhibitors of invasion (Fig. 5a). At 10 nM, 2G10 inhibited about 30% of invasion of MDA-MB-231 cells, and 3C6 inhibited about 14% of invasion. At twenty-times less antibody, 2G10 inhibited about 13% of invasion of MDA-MB-231 cells, and 3C6 inhibited about 8% of invasion. 2G10 and 3C6 also had a pronounced effect on the clonogenic survival of treated MDA-MD-231 cells (Fig. 5b). A concentration of 100 nM for both antibodies resulted in clonal survival below 40%. A high-dose monotherapy study was then initiated in MDA-MB-231 xenograft mice using 2G10, 3C6 and A11 matched isotype control antibody dosed at 30 mg/kg (Fig 5c). The antibodies, and saline control, were administered i.v. to the mice starting on day 3. After four doses a week apart, a statistically significant inhibition of tumor growth compared to the saline control and A11 was observed in the groups treated with 2G10 and 3C6 by day 35. Twenty-five days after the last injected dose, the 2G10 treated group displayed no growth with a mean volume of 140.48 mm^3. The therapeutic benefit observed early on in the 3C6 treated group was diminshed by day 49 with an average tumor volume of nearly 600mm^3.

2G10 was investigated as a radioimmunotherapeutic because of its long *in vivo* half-life and favorable tumor retention properties compared to 3C6. RIT, as with antibody imaging, requires a small amount of material compared to monotherapy. A monotherapy dose at 30 mg/kg for one animal would require 500 μg of 2G10 while an RIT agent would only require 2μg of material. 2G10 was radiolabeled with the therapeutic β particle-emitting radionuclide ^{177}Lu for RIT. A radioactive MTT assay with ^{177}Lu-2G10 and ^{177}Lu-A11 demonstrated that a dose of 50μCi of ^{177}Lu-2G10 resulted in the preferential killing of MDA-MB-231 cells, but not MCF-7 cells (Fig. 5d). Unlabeled 2G10, at a mass used for RIT, was not toxic to either cell line. ^{177}Lu-A11 did show some toxicity in MDA-MB-231 cells, but the level was similar to MCF-7 suggesting that it was due to the inherent toxicity of the isotope and antibody diffusion, rather than targeted localization of the radionuclide. ^{177}Lu-2G10, and a low monotherapy dose of 2G10 (4mg/kg), were evaluated in MDA-MB-231 xenografts. A 150μCi dose of ^{177}Lu-2G10, fractionated into two equivalent doses of 75μCi (2.5μg/dose) two weeks apart, was used for the study. In addition to less myelotoxicity, fractionated dosing allows for a greater total dose to be administered, thus compensating for *in vivo* IgG clearance, and the radionuclide decay. At days 7 and 21, the mice were injected with saline control, 75μCi of ^{177}Lu-2G10, 75μCi of ^{177}Lu chelated to EDTA–to represent non-targeted ^{177}Lu- or 2G10 (4mg/kg) (Fig. 5e). Mice treated with ^{177}Lu-2G10 had marked tumor regression starting after the first dose and the emission of gamma photon by ^{177}Lu decay allowed them to be imaged during the course of treatment (Supplmental Fig. S6). After 35 days, the ^{177}Lu-2G10 treated mice had tumor mean volumes

of 50 mm^3 whereas the tumor volumes of the control arms (saline and ^{177}Lu-EDTA) increased to greater than 1000 mm^3. The tumors of the ^{177}Lu-2G10 group were undetectable at day 49 and none of the tumors of that group (10/10) had recurred by day 84. Despite a much smaller injected mass (4mg/kg versus 30mg/kg) and decreased dosing frequency, the low dose 2G10 monotherapy was effective at mitigating tumor growth with only a three-fold tumor volume increase by day 49.

Discussion

Several groups have shown that uPAR expression in breast tumor tissue is highly correlated with aggressive phenotypes (12, 25). Aberrant uPAR expression is typically seen concomitantly with that of uPA and PAI-1. *In vitro* studies of the PAS utilize particularly aggressive TNBC cell lines as model systems, and several groups have found that simultaneous uPAR and Her2 over-expression effected a higher degree of tumor aggressiveness (13, 26). Interestingly, when non-aggressive breast cancer cells were cultured under hypoxic conditions, uPAR over-expression and a subsequent aggressive phenotype were observed (14). Furthermore, there is an inverse relationship between uPAR expression in breast cancer and the efficacy of tamoxifen in treatment (11). This is corroborated by our finding that tamoxifen-resistant breast cancer cells have a marked increase in PAS component expression. These studies highlight the potential importance of uPAR in cancer cell proliferation and invasion. Internal and external stresses on the tumor may activate pathways leading to uPAR over-expression and subsequent phenotypic changes that help cancer cells escape unfavorable milieus.

Here, the ability of 2G10 and 3C6, two human recombinant anti-uPAR antagonistic antibodies, to bind to uPAR over-expressing breast cancer cells *in vitro*, and target these cells *in vivo*, is described. Previous agents directed towards uPAR have met with mixed results as imaging agents. Antagonistic peptides of uPAR have been used for PET imaging, but poor affinity and limited bioavailability have limited their further development and clinical translation (27). One antibody-based strategy targeting rat uPAR with a ^{125}I labeled probe showed little tumor accumulation that was likely due to the enhanced permeation and retention (EPR) effect and not selective targeting (28). Our data suggest that 2G10 and 3C6 localization in the tumor models was the direct result of uPAR binding and not simply due to the EPR effect or other hemodynamic forces. Three-dimensional SPECT/CT imaging confirmed that 2G10 and 3C6 labeled with ^{111}In permeated the MDA-MB-231 tumors (i.e. they did not pool in the vascularized periphery of the tumor) and that this signal was as robust and long-lived as other antibody probes in clinical development, although ^{111}In-2G10 had more favorable pharmacokinetic properties than ^{111}In-3C6 (29, 30).
Enhanced ^{111}In-3C6 clearance was observed as evident by increased hepatic uptake and a decreased T/B ratio. The decreased uptake by 3C6 could be explained by its lower affinity for uPAR or epitope occlusion. The epitope occlusion argument is plausible - integrin is more abundant on the cell surface compared to uPAR and uPA binding is believed to cause a conformational change in the integrin binding region (31).

Using the MDA-MB-231 CDM model, ^{111}In-labeled 2G10 and 3C6 detected soft-tissue and osseous metastatic lesions. While this is the first such time that a uPAR-targeted antibody has been used to detect lesions like these, the imaging results highlight the potential sensitivity of uPAR SPECT probes in detecting metastases. Furthermore, with this model, it was possible to compare our biomarker-targeted imaging approach with the standard of care metabolic imaging approach for breast cancer, FDG-PET. We found that 2G10 and 3C6 detected more MDA-MB-231 lesions than FDG-PET. Not all tumor cells take up ^{18}FDG, and FDG-PET is known to produce false positive signals – especially in inflamed tissue around the tumor (32). Given the caveats of FDG-PET, we hypothesized that this ^{18}FDG

uptake shown in Figure 4c arose from inflamed tissue surrounding the lesion. In Figure 4c, the ^{18}FDG-avid cells did not bioluminesce, and subsequent studies showed that ^{111}In-2G10 did not localize to sites of inflammation (Suppl. Figure S7). In this study, however, FDG-PET detected two lesions that ^{111}In-2G10 did not (Suppl. Figure S8). The fact the uPAR probes and ^{18}FDG identified different tumors derived from the same cell line highlights the impact of microenvironment on tumor heterogeneity, and how it can influence the ability to comprehensively diagnose and treat breast cancer. While further investigation is needed to understand the basis for this heterogeneity, these results suggest that a combined diagnostic approach, using both biomarkers and metabolic targets, can identify a wider array of lesions than by using any singular imaging agent

A corollary to anti-uPAR IgG localization in tumors is the potential therapeutic benefit resulting from antibody targeting of uPAR. Attempts previously to target uPAR for therapeutic benefit have again met with mixed success. An antibody purported to disrupt the uPAR/uPA system was used to elicit a therapeutic effect in a syngeneic model of rat breast cancer; however, its specificity to uPAR, as well as antagonistic characteristics, were not confirmed (28). Another group demonstrated that concomitant treatment of xenograft tumor-bearing mice with an anti-uPAR antibody and the nucleoside analog gemcitabine effected a stronger therapeutic outcome that treatment with either agent alone (33). Using radiotherapy, uPAR has been targeted with peptides and recombinant proteins. The antagonistic peptide used to image uPAR previously, demonstrated little therapeutic effect and low tumor uptake in a colon cancer model when labeled with ^{177}Lu (34). In a TNBC model, Barry et. al used a recombinant version of PAI-2, an uPA inhibitor expressed during pregnancy, labeled with α-emitting isotope ^{213}Bi to target the uPA/uPAR system (35). This approach worked well against small pre-angiogenic clusters of cells and reduced tumor growth *in vivo. In vitro* studies found that our uPAR antibodies affected cell invasion and clonogenic survival, suggesting potential therapeutic benefit *in vivo*. As a monotherapy at a high dose, 2G10 exhibited a pronounced cytostatic effect and was a more potent therapeutic than 3C6. This difference in therapeutic efficacy is supported by the higher tumor uptake of 2G10 in the imaging studies compared to 3C6 and the longer half-life of 2G10 *in vivo*. Localization of the antibodies to tumors supported the delivery of a therapeutic payload to the tumor site. Here, we found that 2G10 labeled with the therapeutic radionuclide ^{177}Lu demonstrated selective cytotoxicity for uPAR expressing cells *in vitro* and, in an animal study, complete tumor regression. Comparing our *in vivo* work to the studies on ^{213}Bi-PAI-2, found that ^{177}Lu-2G10 was more effective treating established tumors in a TNBC model (35). Currently, RIT is used in the treatment of hematological malignancies with Bexxar and Zevalin as the only two FDA approved agents; however, recent studies have shown that RIT is effective in treating solid tumors such as prostate and colon cancer (36, 37). Our preclinical RIT data suggest that uPAR-targeted RIT agents could be viable options for treating aggressive breast cancers when other therapies have failed. Furthermore, while Bauer et al. indicate that anti-uPAR therapeutics may play a role in potentiating cytotoxic drug responses, our data with 2G10 suggest that disruption of the uPAR/uPA interaction might be a pivotal axis to target in cancers that demonstrate uPAR over-expression. This idea has recently been supported by work where murine antibodies directed towards murine uPA significantly disrupted tumor growth and progression *in vivo* (38). The uPAR antibodies described here are fully human, thus allowing for repeated administration of the antibodies as imaging probes, therapeutics and RIT agents with minimal immunologic side effects.

As with other cancer targets, uPAR expression is, indeed, found on other non-cancerous cells. uPAR's role in effecting cellular migration and proliferation lends it to be important for the function of activated leukocytes, but is not highly expressed in otherwise normal states (39, 40). Additionally, uPAR plays a role in angiogenesis and wound healing (41, 42).

These complications, however, are in the same vein as those for other antibody-based targeted imaging agents and therapeutics. Given the abundance of uPAR on aggressive tumor cells (especially on tumor-associated macrophages and fibroblasts) relative to resting leukocytes and other cells that express uPAR, the data presented here on 2G10 and 3C6 underscore uPAR's potential as a diagnostic and therapeutic target.

Supplementary Material

Refer to Web version on PubMed Central for supplementary material.

Acknowledgments

Financial Support: This work was supported by the Rogers Family Bridging the Gap Award (C.S.C and H.F.V.), NIH grant CA128765 (C.S.C.), NIH NCI grant P50 CA 58207, and the U54 CA 112970 (to J.W.G) and a Department of Defense Postdoctoral Prostate Cancer Award PC094386 (A.M.L)

The authors would like to thank Laura Esserman and Laura vant'Veer for careful reading of the manuscript and useful scientific discussions and Donghui Wang for excellent technical assistance in performing animal studies. This work was supported by the Rogers Family Award (to C.S.C. and H.F.V.) and the National Institutes of Health grant R01 CA128765 (to C.S.C.), National Cancer Institute grant P50 CA 58207, and the U54 CA 112970 (to J.W.G). A.M.L. was supported by a DOD prostate cancer postdoctoral award PC094386. S.D. received predoctoral funding from the Chih Foundation Award, the UC Cancer Research Coordinating Committee and NIH training grant GM008284-25.

References

1. Higgins MJ, Baselga J. Targeted therapies for breast cancer. J Clin Invest. 2011; 121(10):3797–803. [PubMed: 21965336]
2. Heiser LM, Sadanandam A, Kuo WL, Benz SC, Goldstein TC, Ng S, et al. Subtype and pathway specific responses to anticancer compounds in breast cancer. Proc Natl Acad Sci U S A. 2012; 109(8):2724–9. [PubMed: 22003129]
3. Tsang RY, Finn RS. Beyond trastuzumab: novel therapeutic strategies in HER2-positive metastatic breast cancer. Br J Cancer. 2012; 106(1):6–13. [PubMed: 22215104]
4. Nahta R, Esteva FJ. HER-2-targeted therapy: lessons learned and future directions. Clin Cancer Res. 2003; 9(14):5078–84. [PubMed: 14613984]
5. Johnston SR. The role of chemotherapy and targeted agents in patients with metastatic breast cancer. Eur J Cancer. 2011; 47 (Suppl 3):S38–47. [PubMed: 21944023]
6. Largillier R, Ferrero JM, Doyen J, Barriere J, Namer M, Mari V, et al. Prognostic factors in 1,038 women with metastatic breast cancer. Ann Oncol. 2008; 19(12):2012–9. [PubMed: 18641006]
7. Sidenius N, Blasi F. The urokinase plasminogen activator system in cancer: recent advances and implication for prognosis and therapy. Cancer Metastasis Rev. 2003; 22(2–3):205–22. [PubMed: 12784997]
8. Dass K, Ahmad A, Azmi AS, Sarkar SH, Sarkar FH. Evolving role of uPA/uPAR system in human cancers. Cancer Treat Rev. 2008; 34(2):122–36. [PubMed: 18162327]
9. Meijer-van Gelder ME, Look MP, Peters HA, Schmitt M, Brunner N, Harbeck N, et al. Urokinase-type plasminogen activator system in breast cancer: association with tamoxifen therapy in recurrent disease. Cancer Res. 2004; 64(13):4563–8. [PubMed: 15231667]
10. Harbeck N, Kates RE, Schmitt M, Gauger K, Kiechle M, Janicke F, et al. Urokinase-type plasminogen activator and its inhibitor type 1 predict disease outcome and therapy response in primary breast cancer. Clin Breast Cancer. 2004; 5(5):348–52. [PubMed: 15585071]
11. Gelder MEV, Look MP, Peters HA, Schmitt M, Brunner N, Harbeck N, et al. Urokinase-type plasminogen activator system in breast cancer: Association withtamoxifen therapy in recurrent disease. Cancer Research. 2004; 64(13):4563–8. [PubMed: 15231667]
12. Bianchi E, Cohen RL, Thor AT, Todd RF, Mizukami IF, Lawrence DA, et al. The Urokinase Receptor Is Expressed in Invasive Breast-Cancer but Not in Normal Breast-Tissue. Cancer Research. 1994; 54(4):861–6. [PubMed: 8313371]

13. Konecny G, Untch M, Arboleda J, Wilson C, Kahlert S, Boettcher B, et al. Her-2/neu and urokinase-type plasminogen activator and its inhibitor in breast cancer. Clin Cancer Res. 2001; 7(8):2448–57. [PubMed: 11489825]

14. Jo M, Lester RD, Montel V, Eastman B, Takimoto S, Gonias SL. Reversibility of epithelial-mesenchymal transition (EMT) induced in breast cancer cells by activation of urokinase receptor-dependent cell signaling. J Biol Chem. 2009; 284(34):22825–33. [PubMed: 19546228]

15. Duriseti S, Goetz DH, Hostetter DR, LeBeau AM, Wei Y, Craik CS. Antagonistic anti-urokinase plasminogen activator receptor (uPAR) antibodies significantly inhibit uPAR–mediated cellular signaling and migration. J Biol Chem. 2010; 285(35):26878–88. [PubMed: 20501655]

16. van de Vijver MJ, He YD, van't Veer LJ, Dai H, Hart AA, Voskuil DW, et al. A gene-expression signature as a predictor of survival in breast cancer. N Engl J Med. 2002; 347(25):1999–2009. [PubMed: 12490681]

17. van Vliet MH, Reyal F, Horlings HM, van de Vijver MJ, Reinders MJ, Wessels LF. Pooling breast cancer datasets has a synergetic effect on classification performance and improves signature stability. BMC Genomics. 2008; 9:375. [PubMed: 18684329]

18. Darragh MR, Schneider EL, Lou J, Phojanakong PJ, Farady CJ, Marks JD, et al. Tumor detection by imaging proteolytic activity. Cancer Res. 2010; 70(4):1505–12. [PubMed: 20145119]

19. Kang Y, Siegel PM, Shu W, Drobnjak M, Kakonen SM, Cordon-Cardo C, et al. A multigenic program mediating breast cancer metastasis to bone. Cancer Cell. 2003; 3(6):537–49. [PubMed: 12842083]

20. Dalrymple SL, Becker RE, Zhou H, DeWeese TL, Isaacs JT. Tasquinimod prevents the angiogenic rebound induced by fractionated radiation resulting in an enhanced therapeutic response of prostate cancer xenografts. Prostate. 2012; 72(6):638–48. [PubMed: 21837778]

21. Rouzier R, Perou CM, Symmans WF, Ibrahim N, Cristofanilli M, Anderson K, et al. Breast cancer molecular subtypes respond differently to preoperative chemotherapy. Clin Cancer Res. 2005; 11(16):5678–85. [PubMed: 16115903]

22. Calza S, Hall P, Auer G, Bjohle J, Klaar S, Kronenwett U, et al. Intrinsic molecular signature of breast cancer in a population-based cohort of 412 patients. Breast Cancer Res. 2006; 8(4):R34. [PubMed: 16846532]

23. Sotiriou C, Neo SY, McShane LM, Korn EL, Long PM, Jazaeri A, et al. Breast cancer classification and prognosis based on gene expression profiles from a population-based study. Proc Natl Acad Sci U S A. 2003; 100(18):10393–8. [PubMed: 12917485]

24. Hiscox S, Jiang WG, Obermeier K, Taylor K, Morgan L, Burmi R, et al. Tamoxifen resistance in MCF7 cells promotes EMT-like behaviour and involves modulation of beta-catenin phosphorylation. Int J Cancer. 2006; 118(2):290–301. [PubMed: 16080193]

25. Kotzsch M, Bernt K, Friedrich K, Luther E, Albrecht S, Gatzweiler A, et al. Prognostic relevance of tumour cell-associated uPAR expression in invasive ductal breast carcinoma. Histopathology. 2010; 57(3):461–71. [PubMed: 20840675]

26. Meng S, Tripathy D, Shete S, Ashfaq R, Saboorian H, Haley B, et al. uPAR and HER-2 gene status in individual breast cancer cells from blood and tissues. Proc Natl Acad Sci U S A. 2006; 103(46): 17361–5. [PubMed: 17079488]

27. Li ZB, Niu G, Wang H, He L, Yang L, Ploug M, et al. Imaging of urokinase-type plasminogen activator receptor expression using a 64Cu-labeled linear peptide antagonist by microPET. Clin Cancer Res. 2008; 14(15):4758–66. [PubMed: 18676745]

28. Rabbani SA, Gladu J. Urokinase receptor antibody can reduce tumor volume and detect the presence of occult tumor metastases in vivo. Cancer Res. 2002; 62(8):2390–7. [PubMed: 11956102]

29. Smith-Jones PM, Vallabhajosula S, Navarro V, Bastidas D, Goldsmith SJ, Bander NH. Radiolabeled monoclonal antibodies specific to the extracellular domain of prostate-specific membrane antigen: preclinical studies in nude mice bearing LNCaP human prostate tumor. J Nucl Med. 2003; 44(4):610–7. [PubMed: 12679407]

30. Schneider DW, Heitner T, Alicke B, Light DR, McLean K, Satozawa N, et al. In vivo biodistribution, PET imaging, and tumor accumulation of 86Y-and 111In-antimindin/RG-1,

engineered antibody fragments in LNCaP tumor-bearing nude mice. J Nucl Med. 2009; 50(3):435–43. [PubMed: 19223400]

31. Mertens HD, Kjaergaard M, Mysling S, Gardsvoll H, Jorgensen TJ, Svergun DI, et al. A flexible multidomain structure drives the function of the urokinase-type plasminogen activator receptor (uPAR). J Biol Chem. 2012
32. Adejolu M, Huo L, Rohren E, Santiago L, Yang WT. False-positive lesions mimicking breast cancer on FDG PET and PET/CT. AJR Am J Roentgenol. 2012; 198(3):W304–14. [PubMed: 22358030]
33. Bauer TW, Liu W, Fan F, Camp ER, Yang A, Somcio RJ, et al. Targeting of urokinase plasminogen activator receptor in human pancreatic carcinoma cells inhibits c-Met- and insulin-like growth factor-I receptor-mediated migration and invasion and orthotopic tumor growth in mice. Cancer Res. 2005; 65(17):7775–81. [PubMed: 16140945]
34. Persson M, Rasmussen P, Madsen J, Ploug M, Kjaer A. New peptide receptor radionuclide therapy of invasive cancer cells: in vivo studies using 177Lu-DOTA-AE105 targeting uPAR in human colorectal cancer xenografts. Nucl Med Biol. 2012; 39(7):962–9. [PubMed: 22739362]
35. Allen BJ, Tian Z, Rizvi SM, Li Y, Ranson M. Preclinical studies of targeted alpha therapyfor breast cancer using 213Bi-labelled-plasminogen activator inhibitor type 2. Br J Cancer. 2003; 88(6):944–50. [PubMed: 12644835]
36. Morris MJ, Divgi CR, Pandit-Taskar N, Batraki M, Warren N, Nacca A, et al. Pilot trial of unlabeled and indium-111-labeled anti-prostate-specific membrane antigen antibody J591 for castrate metastatic prostate cancer. Clin Cancer Res. 2005; 11(20):7454–61. [PubMed: 16243819]
37. Baechler S, Hobbs RF, Jacene HA, Bochud FO, Wahl RL, Sgouros G. Predicting hematologic toxicity in patients undergoing radioimmunotherapy with 90Y-ibritumomab tiuxetan or 131I-tositumomab. J Nucl Med. 2010; 51(12):1878–84. [PubMed: 21098795]
38. Lund IK, Rasch MG, Ingvarsen S, Pass J, Madsen DH, Engelholm LH, et al. Inhibitory Monoclonal Antibodies against Mouse Proteases Raised in Gene-Deficient Mice Block Proteolytic Functions in vivo. Front Pharmacol. 2012; 3:122. [PubMed: 22754528]
39. Politis I, Zavizjon B, Cheli F, Baldi A. Expression of urokinase plasminogen activator receptor in resting and activated bovine neutrophils. J Dairy Res. 2002; 69(2):195–204. [PubMed: 12222798]
40. Jardi M, Ingles-Esteve J, Burgal M, Azqueta C, Velasco F, Lopez-Pedrera C, et al. Distinct patterns of urokinase receptor (uPAR) expression by leukemic cells and peripheral blood cells. Thromb Haemost. 1996; 76(6):1009–19. [PubMed: 8972026]
41. D'Alessio S, Gerasi L, Blasi F. uPAR-deficient mouse keratinocytes fail to produce EGFR-dependent laminin-5, affecting migration in vivo and in vitro. J Cell Sci. 2008; 121(Pt 23):3922–32. [PubMed: 19001498]
42. Smith HW, Marshall CJ. Regulation of cell signalling by uPAR. Nat Rev Mol Cell Biol. 2010; 11(1):23–36. [PubMed: 20027185]

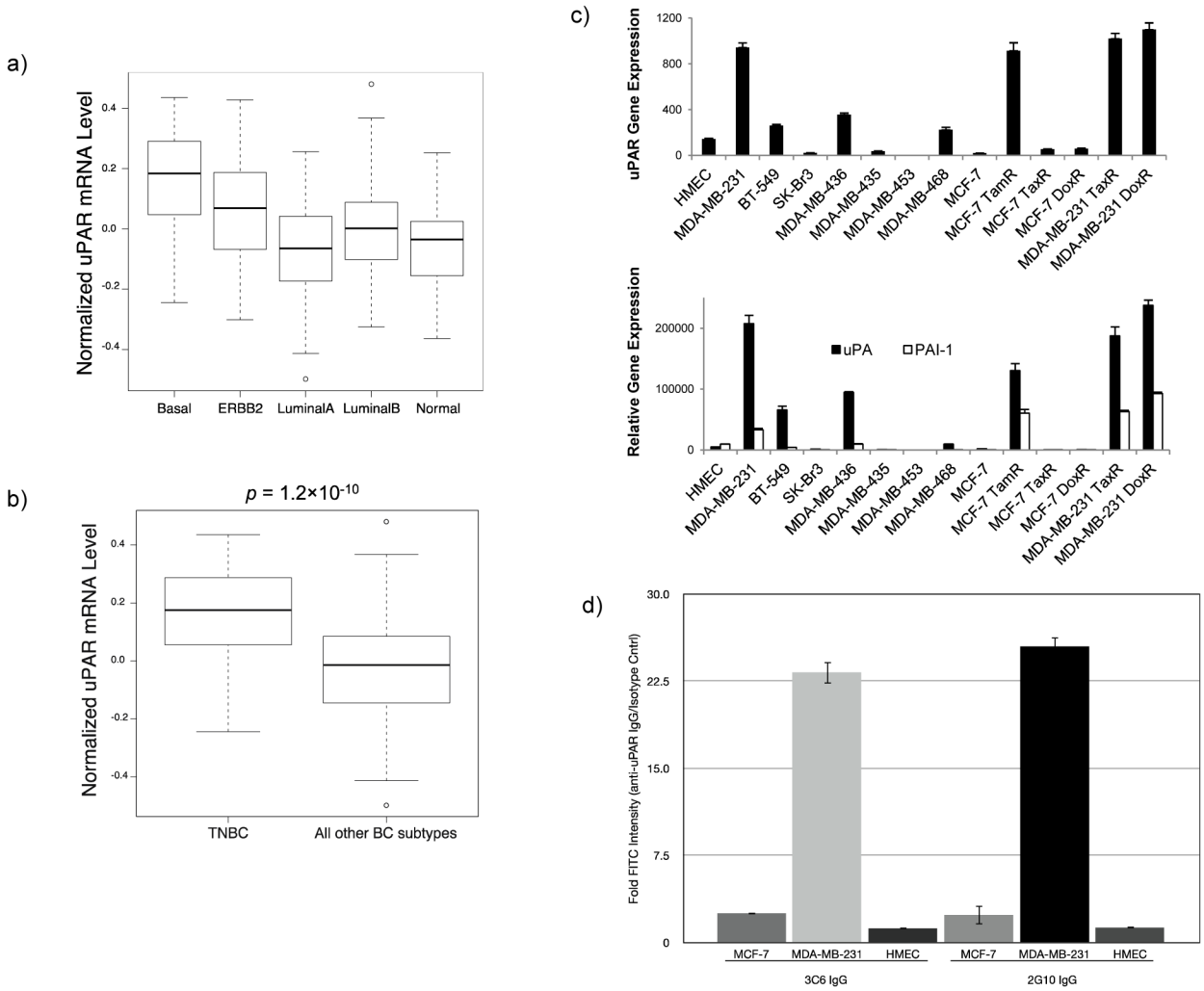

Figure 1.

High uPAR mRNA levels correlate with a TNBC phenotype. **(a)** Established breast cancer subtypes in the NKI dataset were probed for uPAR mRNA levels using a non-parametric Wilcoxian test. Basal (BLBC) was identified as having the highest levels of uPAR mRNA. **(b)** uPAR mRNA levels were probed in two groups, TNBC and all over breast cancer phenotypes. **(c)** mRNA levels of the PAS were analyzed using quantitative RT-PCR in breast cancer cell lines and normal human mammary epithelial cells (HMECs). **(d)** uPAR staining of MDA-MB-231, MCF-7, and HMEC cells. Stronger staining with 2G10 and 3C6 IgG was seen on MDA-MB-231 cells, correlating with mRNA data, and reflected higher uPAR protein expression in these cells.

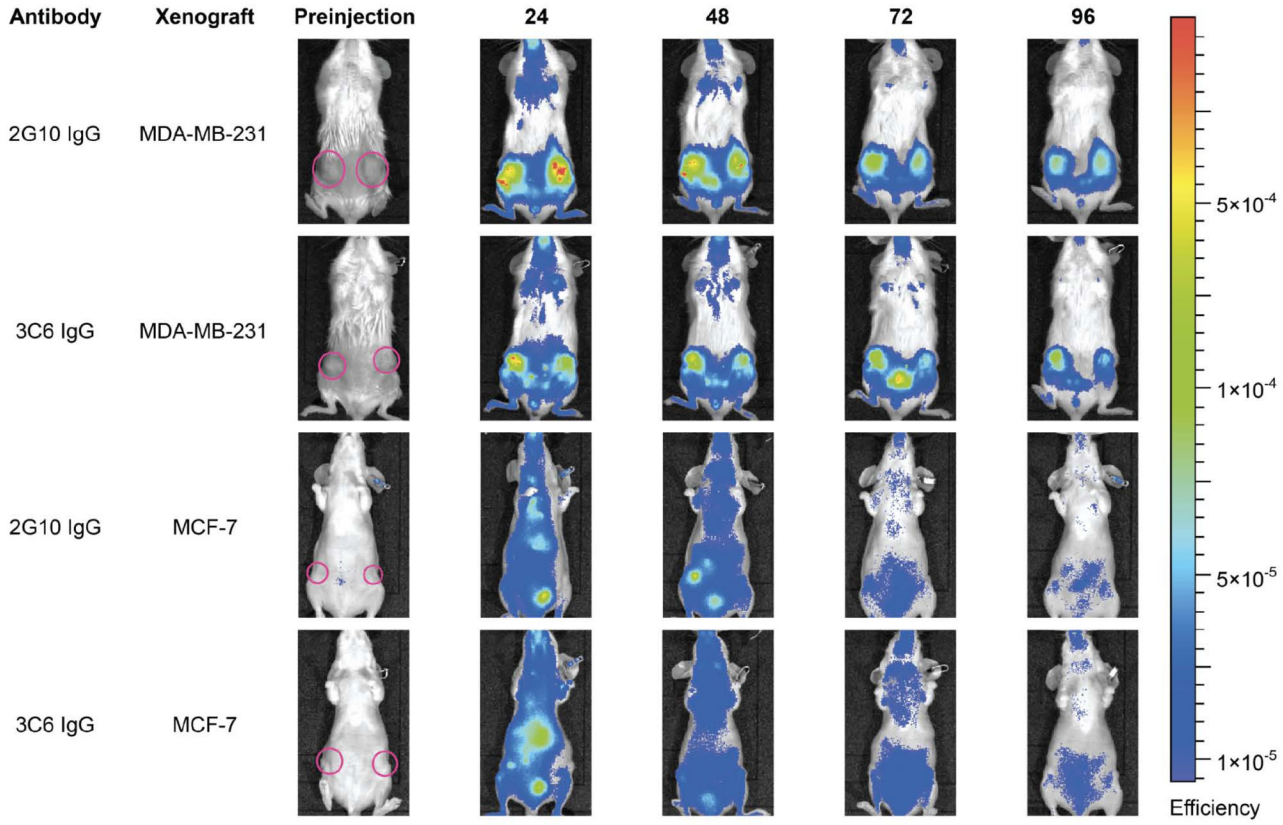

Figure 2.

2G10 and 3C6 accumulate in MDA-MB-231 xenograft tumors using near-infrared optical imaging. SCID mice bearing MDA-MB-231 and MCF-7 xenograft tumors (circled in pink in the pre-injection panels) were injected with ~2 nanomoles of AlexaFluor 680-labeled 2G10 and 3C6. After injection, images were obtained every 24 hours for four days as indicated. Weak non-specific signals were observed in MCF-7 tumor-bearing mice injected with 2G10 and 3C6. Four tumor-bearing mice were used for each sample set.

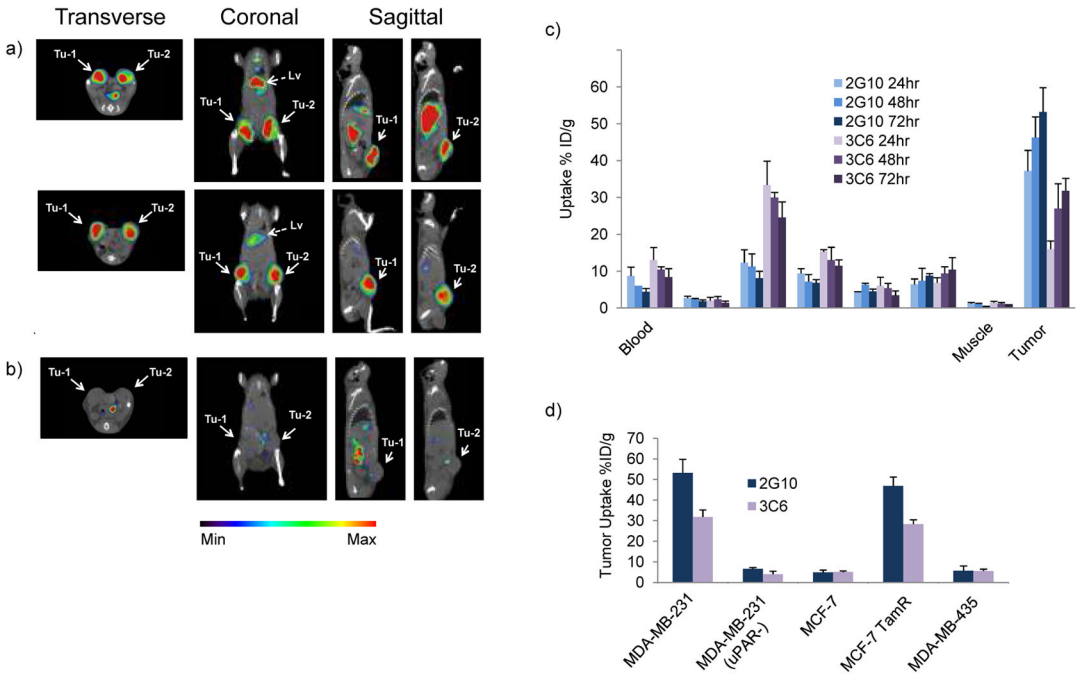

Figure 3.

SPECT/CT imaging reveals that ^{111}In-2G10 and ^{111}In-3C6 localize to the tumor interior of the MDA-MB-231 xenograft preferentially. SCID mice bearing bilateral MDA-MB-231 and MCF-7 orthotopic xenograft tumors were injected with ^{111}In-DOTA-labeled 3C6 and 2G10. Each animal (n=3/xenograft/probe) received an injected dose of 2.5ug of radiolabeled antibody corresponding to an activity of 250 – 350 μCi. (**a**) Transverse, coronal and sagittal views of co-registered SPECT/CT images depict ^{111}In-3C6 (upper) and ^{111}In-2G10 (lower) localized to the two MDA-MB-231 tumors (Tu-1 and Tu-2). Secondary hepatic uptake (Lv) is visible with both antibodies, but a weaker signal was observed for ^{111}In-2G10. (**b**) Reconstructed views of an MCF-7 xenograft injected with ^{111}In-2G10 does not show tumor uptake in either of the two tumors implanted. These data agree with the NIR finding and previous data indicating a lack of uPAR expression in MCF-7 cells. The images presented here were acquired 72 hours post-injection and are representative of n = 3 mice imaged/antibody/xenograft. (**c**) Biodistribution study of ^{111}In-2G10 and ^{111}In-3C6 in MDA-MB-231 xenograft mice (n = 4) at three time points injected with 50μCi of probe. Probe localization is expressed %ID/g. (**d**) Tumor uptake of the probes at 72hrs in animals bearing MDA-MB-231 (n = 4), MDA-MD-231 (uPAR-) (n = 3), MDA-MB-435 (n = 3), MCF-7 (n = 3) and MCF-7 TamR (n = 3) xenografts.

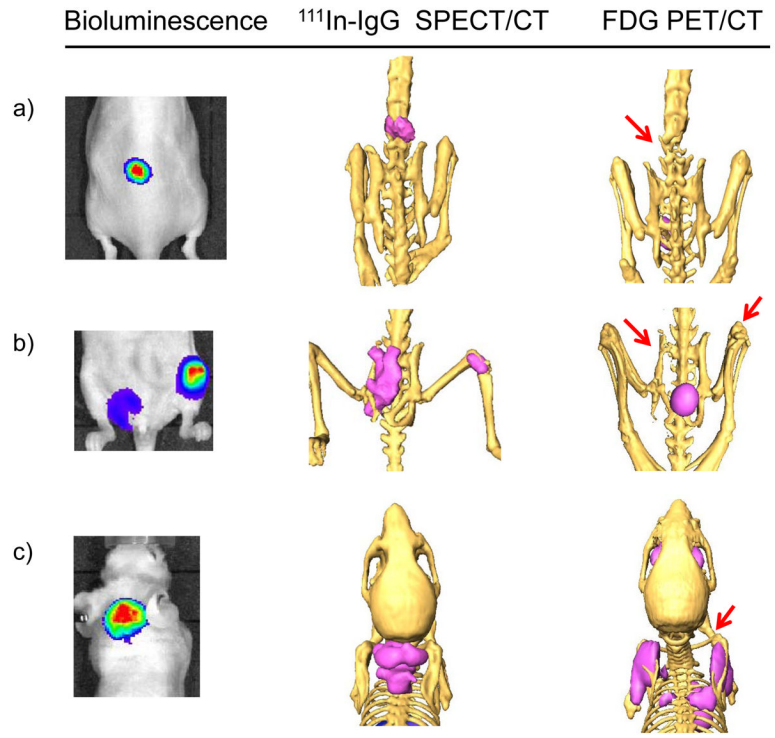

Figure 4.

^{111}In labeled anti-uPAR antibodies specifically target metastatic lesions in the MDA-MB-231 CDM model. Metastatic colonies formation was observed using bioluminescence imaging (BLI) following the injection of D-luciferin. Mice demonstrating strong BLI signals were fasted overnight and imaged with FDG-PET/CT (150–200 μCi) 60 minutes post-injection. 24 hours after FDG-PET/CT, the mice were injected with the ^{111}In-labeled uPAR antibodies (275–300 μCi). The SPECT/CT images shown here were acquired 72 hours post-injection. The SPECT/CT and PET/CT images depicted are 3-dimensional volume rendering of the nuclear imaging data overlaid onto surface-rendered CT data. (**a**) A SPECT/CT image showed that ^{111}In-3C6 localized to an osseous metastatic lesion located in the spine that went undetected by FDG-PECT/CT. (b) Osteolytic lesions in the illium and knee were detected with SPECT/CT using ^{111}In-2G10 which prevents uPA binding to the receptor. (**c**) Bioluminescent tumor cells were found by ^{111}In-2G10 at the base of the skull. The bioluminescent cells were found to be non-FDG avid, however, FDG uptake was observed in inflammatory cells surrounding the lesion. Inflammation induced FDG avidity was confirmed in an inflammatory mouse model that showed pronounced FDG uptake, but no ^{111}In-2G10 localization *in vivo* (Supplementary Fig. S6).

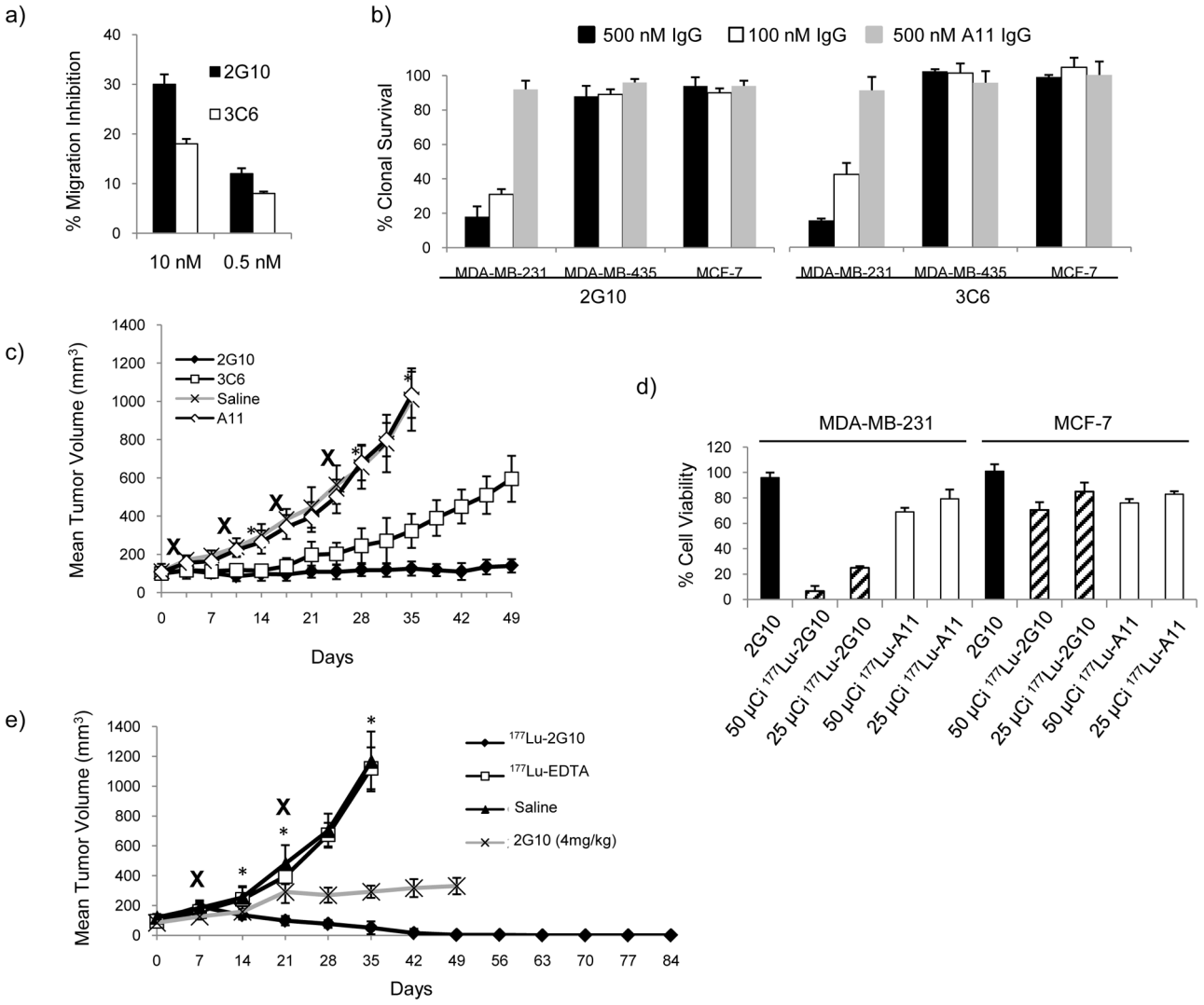

Figure 5.

The therapeutic efficacy of 3C6 and 2G10 *in vitro* and *in vivo*. (**a**) The effect of 3C6 and 2G10 on the Matrigel-coated transwell migration of MDA-MB-231 cells. Media containing 5% FBS was added to the bottom chamber, and the migration of cells was monitored over 24 hours in a fluorescence plate reader. **(b)** The effect of the three antibodies 2G10, 3C6 and A11 on the clonogenic survival of uPAR expressing MDA-MB-231 cells and non-expressing MDA-MB-435 and MCF-7 cells. **(c)** Tumor growth of MDA-MB-231 xenograft mice treated with a high dose (30mg/kg) of 2G10, 3C6, A11 matched isotype control IgG and saline control. Mice (n = 10/group) were dosed four times over the course of the study as denoted by (X). Asterisk denotes indicated $p < 0.05$ via a Student's t-test. **(d)** The targeted cytotoxicity of ^{177}Lu-2G10 on MDA-MB-231cells compared to MCF-7 cells as measured by MTT assay. MDA-MB-231 and MCF-7 cells in a 96 well plate were treated for 96 hours with unlabeled 2G10 (2.5μg), 50μCi and 25μCi of ^{177}Lu-2G10 (2.5ug) or A11 (2.5μg). **(e)** The therapeutic effect of ^{177}Lu-2G10 was tested in SCID mice bearing MDA-MB-231 tumors. Mice (n = 10/group) were treated with ^{177}Lu-2G10 (75μCi – 2.5μg), ^{177}Lu-EDTA (75μCi), saline and 2G10 (4mg/kg) at the indicted time points, (X) denotes dosing. Asterisk denotes indicated $p < 0.05$ via a Student's t-test.

Table 1

Calculated KD values of 2G10 and 3C6 Fab and IgG using SPR and MDA-MB-231 cells using flow cytometry.

Antibody Construct	K_D (SPR) (mol/L)	K_D (MDA-MB-231 cells) (mol/L)
2G10 Fab	10×10^{-9}	$50 \pm 5 \times 10^{-9}$
3C6 Fab	50×10^{-9}	$800 \pm 115 \times 10^{-9}$
2G10 IgG	2×10^{-12}	$2 \pm 0.5 \times 10^{-9}$
3C6 IgG	230×10^{-12}	$5 \pm 0.5 \times 10^{-9}$